Poly (Diallyldimethylammonium Chloride) Functionalized Reduced Graphene Oxide Based Electrochemical Sensing Platform for Luteolin Determination

Li Fu[1], Yuhong Zheng[1,] and Aiwu Wang[2]*

[1] Institute of Botany, Jiangsu Province and Chinese Academy of Sciences, Nanjing Botanical Garden, Mem. Sun Yat-Sen, Nanjing 210014 P. R. China
[2] Center of Super-Diamond and Advanced Films (COSDAF) and Department of Physics and Materials Science, City University of Hong Kong , Hong Kong SAR, P. R. China
[*]E-mail: yuhongzhengcas@gmail.com

We describe the development of a sensitive electrochemical luteolin sensor based on poly (diallyldimethylammoniumchloride) (PDDA) functionalized reduced graphene oxide (PDDA-RGO). The PDDA-RGO sheets were characterized by SEM, XRD, Raman spectroscopy, UV-vis spectroscopy and FTIR. The results indicate the PDDA-RGO sheets exhibit excellent dispersity and conductivity. Electrochemical studies showed that the PDDA-RGO modified glassy carbon electrode (GCE) could greatly enhance the electrocatalytic activity towards the redox of luteolin. A series of experimental conditions including the pH, accumulation potential and time were optimized. The proposed sensor exhibited a wide detection range (0.001 to 10μM) with a detection limit of 0.001 μM (S/N = 3). Moreover, the proposed electrochemical sensor has also been successfully applied to determination of luteolin in thyme sample.

1. INTRODUCTION

Luteolin (3',4',5,7-tetrahydroxy-flavone) is one of the most bioactive flavonoids that exists in many types of plants such as parsley, thyme, peppermint artichoke, perilla leaf and chamomile tea [1, 2]. Studies have shown that luteolin has a broad range of biochemical and pharmacological properties, including anti-platelet, anti-ulcer, anti-inflammatory, cardiovascular protection, anti-bacteria and anti-virus properties [3-7]. Recent studies have further shown that it could enter the cellular nuclei and suppress the oxidative damage of DNA, lipids, proteins, and carbohydrates [8, 9]. Therefore, control

and monitor the dosage of luteolin is very important in the clinical field. Up to now, a great deal of methods have been reported for the determination of luteolin in flavonoids, including high-performance liquid chromatography (HPLC) [10-12], capillary electrophoresis [13, 14], spectrophotometry [15], gas chromatography (GC) [16] etc. Although these methods are highly capable for determining luteolin, but they are time-consuming, expensive and required skilled operator, which cannot be applied for on-line or field monitoring. In order to avoid these problems, and since luteolin is an electroactive compound, electrochemical determination is an alternative approach for luteolin detection due to its sensitivity, accuracy, lower cost and simplicity. So far, only several studies have been carried out for electrochemical determination of luteolin [17-22]. For example, Tesio and co-workers reported [18] electrochemical detection of luteolin based on a glassy carbon electrode (GCE) modified with multiwalled carbon nanotubes dispersed in low molecular weight polyethylenimine. Zeng and co-workers [21] demonstrated the detection of luteolin based on a macroporous carbon modified GCE. However, we think the development of novel electrode modified materials with excellent conductivity, catalytic activity and stability still remains a challenge.

Graphene sheets, a two-dimensional single-atom-thick conjugated carbon network, have attracted a great deal of interest due to its extraordinary properties, such as excellent electronic conductivity, large specific surface area and potential applications in biosensors [23-27]. However, most of the graphene used in this procedure is in its reduced form from graphene oxide (GO) prepared by the oxidation of graphite. The reduced graphene oxide (RGO) is prone to irreversible spontaneous agglomeration, which highly limits its applications and performances. To overcome this problem, poly (diallyldimethylammoniumchloride) (PDDA) has been studied for functionalizing GO to a solution-processable RGO [28].

In this study, polyelectrolyte PDDA functionalized graphene nanosheet (PDDA-RGO) was prepared via a facial wet chemical route. Subsequently, a sensitive electrochemical sensor for luteolin detection was fabricated based on the PDDA-RGO modified GCE. The result PDDA-RGO nanosheet was characterized by a series of techniques. Several factors affecting the electrocatalytic performances of the proposed luteolin sensor were also further optimized. Due to the large surface area and good conductivity of PDDA-RGO, as-fabricated sensor exhibited excellent electrocatalytic activity towards luteolin determination with wide linear range and low detection limit.

2. EXPERIMENTS

2.1 Chemicals and materials

Luteolin, synthetic graphite (average particle diameter <20 μm), poly(diallyldimethylammonium chloride) (20 wt% in water) (PDDA) and hydrazine hydrate (N_2H_4 50-60 % in water) were purchased from Sigma-Aldrich. Other chemicals were of analytical reagent grade and used without further purification. Milli-Q water (18.2 MΩ cm) was used throughout the experiments.

2.2 Synthesis of PDDA-RGO nanosheet

　　　　Graphene oxide (GO) was prepared with the modified Hummers method with little modification [27, 29, 30]. PDDA-RGO was prepared by a facial wet chemical method according to the literatures with some modifications [28, 31]. Briefly, 5 mg GO was dispersed in 10 mL water and then 2 mL PDDA (0.5 wt.%) was added. The aggregation of dispersion was resolved by 10 min sonication. Then 0.1 mL of N_2H_4 was added into dispersion, and the mixture was heated to 90 °C for 30 min. After cool down, the mixture was centrifuged three times followed by washing process for removing excess PDDA and N_2H_4. Finally, the PDDA-RGO was re-dispersed into 10 mL water to obtain 0.5 mg/mL PDDA-RGO. RGO without PDDA functionalization was also prepared using a similar method expect adding PDDA.

2.3 Characterization

　　　　The morphology of as-synthesized nanocomposite was observed using a ZEISS, SUPRA 55 field emission scanning electron microscopy (FESEM) measurements. The crystal phase information of sample was characterized from 5° to 80° in 2θ by a XRD with Cu Kα ($\lambda = 0.1546$ nm) radiation (D8-Advanced, Bruker). The optical analysis was obtained by UV-vis spectrophotometer (Perkin Elmer Lambda 950). Fourier transform infrared spectroscopy (FTIR) was recorded on a Bruker Vertex 70 spectrometer (2 cm^{-1}). Raman spectroscopy was performed at room temperature using a Raman Microprobe (Renishaw RM1000) with 514 nm laser light.

2.4 Electrode preparation

　　　　A glassy carbon electrode (GCE, diameter of 3 mm) was successively polished with 0.3 and 0.05 μm Al_2O_3 slurry on an abrasive cloth and thoroughly cleaned with ethanol and distilled water under ultrasonication. For the electrode surface modification, 5 μL of catalyst dispersion (1 mg/mL) was dropped onto the GCE and dried at room temperature. Electrochemical measurements were performed on a CHI660D electrochemical workstation (USA), using a three electrode system. A platinum wire was used as the auxiliary electrode and an Ag/AgCl (3M KCl) as the reference electrode. All electrochemical measurements were carried out at room temperature.

3. RESULTS AND DISCUSSION

3.1 Characterization of PDDA-RGO nanosheet

　　　　The surface morphology of the resulting samples were observed by SEM. Figure 1A-B display the typical SEM images of RGO and PDDA-RGO nanosheets. It can be seen that the RGO sheets (Figure 1A) show a stack layered structure, thus the surface area of RGO should be greatly decreased.

In contrast, PDDA-RGO sheets show a well dispersity with some thin layer caused wrinkles. Therefore, the surface PDDA functionalization could retain a large surface area of RGO.
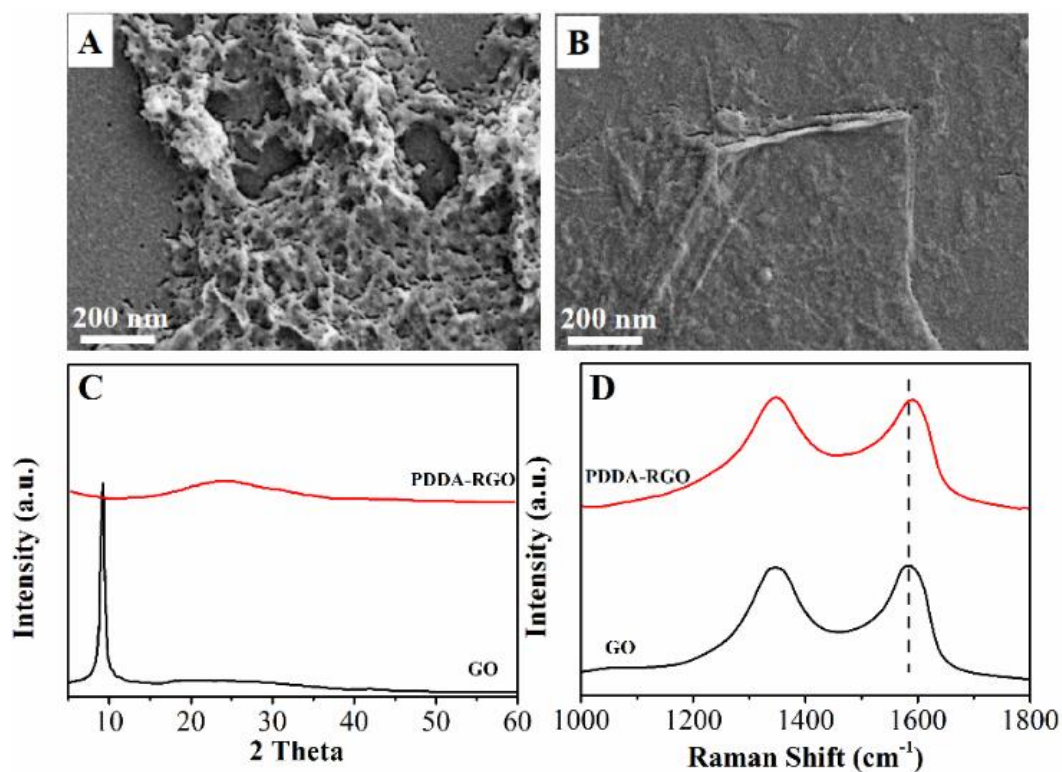

Figure 1. SEM images of (A) RGO and (B) PDDA-RGO. (C) XRD patterns and (D) Raman spectra of GO and PDDA-RGO.
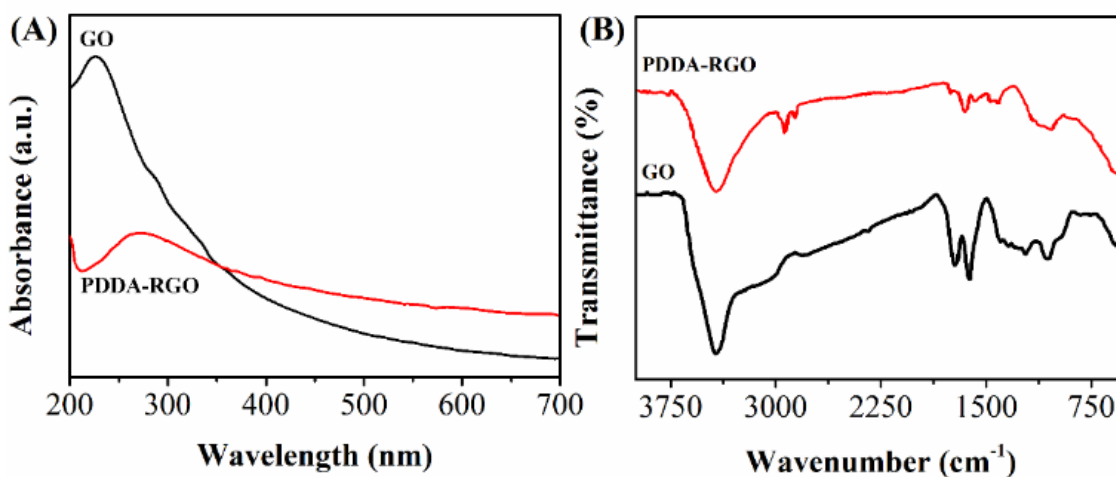

Figure 2. (A) UV-vis spectra and (B) FTIR spectra of GO and PDDA-RGO.

Figure 1 C shows the crystalline structure of GO and PDDA-RGO nanosheet. The XRD pattern of pure GO exhibits a characteristic (002) peak at 11.0° with a *d*-spacing value of 0.82 nm [32]. After

reduction process, the peak shifts to 23.2°, which is the reflection of removal of oxygen-containing functional groups [33, 34], indicating the successful occurrence of the reduction process.

Figure 1D shows the Raman spectra of GO and PDDA-RGO. As expected, the spectrum of GO display two characteristic bands at 1570 and 1340 cm^{-1}, corresponding to the graphite (G band, first-order scattering of E_{2g} phonons by sp^2 carbon atoms) and diamondoid (D band, breathing mode of κ-point photons of A_{1g} symmetry) bands, respectively [35]. The intensity ratio between D band and G band (I_D/I_G) is found to be increased in PDDA-RGO nanosheet with compare to GO, suggesting a decrease of sp^2 domain induced by the N_2H_4 reduction [36]. Moreover, after PDDA surface functionalization, the G band has a small shift from 1570 to 1592 cm^{-1} due to the electron transfer from RGO to the adsorbed PDDA [25, 37-40].

UV−vis spectroscopy was also used for confirming the reduction process. In Figure 2A, the UV−vis spectrum of GO aqueous dispersion displays a strong band at 228 nm and a shoulder peak at about 317 nm, which assign to the π−π* transitions of aromatic C─C bonds and n−π* transitions of C=O bonds [41], while for the PDDA-RGO, the absorption peak red shifts to 272 nm and the absorption increases in visible range, suggesting that GO was completely reduced and the electronic conjugation within the RGO sheets was restored upon N_2H_4 reduction [42].
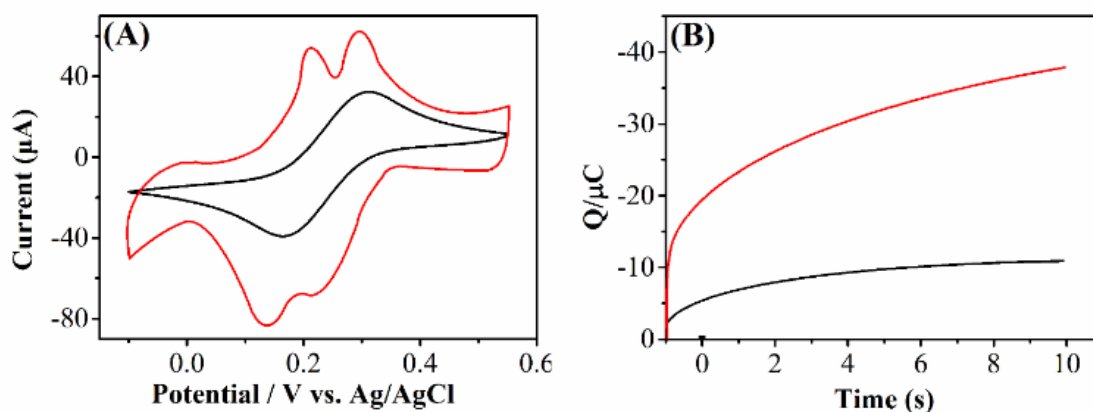

Figure 3. (A) Cyclic voltammograms spectra of bare GCE (black) and PDDA-RGO/GCE (red) in 1.0 mM $K_3[Fe(CN)_6]$ containing 0.1 M KCl. Scan rate 50 mV/s. (B) Chronocoulometric curves of the 1.0 mM $K_3[Fe(CN)_6]$ containing 0.1 M KCl at the bare GCE (balck) and PDDA-Gr/GCE (red).

FTIR was employed for analysing the surface functionalization process of GO. Figure 2B displays the FTIR spectra of GO and PDDA-RGO nanosheets. As expected, the spectrum of GO shows peaks at 1705 cm^{-1}, 1592 cm^{-1}, 1393 cm^{-1} and 1025 cm^{-1}, which are assigned to the C═O stretching of COOH groups, C=C vibrations, C─OH stretching vibrations and C─O vibrations from alkoxy groups, respectively [24, 43-45]. After reduction process, these peaks decrease dramatically and some of them disappeared entirely, further indicate that most of the oxygen-containing functional groups of GO were removed during the reduction process. Moreover, the spectrum of PDDA-RGO also exhibits

bands at 2925, 1642 and 1467 cm^{-1}, belonging to the characteristic bands of PDDA [46]. Therefore, the results indicate the RGO surface has been successfully functionalized with PDDA.

The electrochemical characterization of PDDA-RGO nanosheets was also carried out. Figure 3A shows cyclic voltammograms (CVs) obtained at bare GCE (black), PDDA-RGO/GCE (red) in 1 mM K$_3$Fe(CN)$_6$ containing 0.1 M KCl. It can be seen that the PDDA-RGO/GCE exhibits a much higher current response compared with bare GCE. It could ascribe to the large surface area and the positive surface charge of PDDA-RGO, which provide more active site and electrostatic attraction for Fe(CN)$_6$$^{3-}$ adsorption [28]. Beside the redox peak of Fe(CN)$_6$$^{3-}$, the CV of PDDA-RGO/GCE also exhibits another couple peaks at 0.21 and 0.23 V corresponding to the redox peaks of PDDA. This is consistent with reported work of others [28, 33].

Chronocoulometry investigation was carried out for analyzing the electrochemically effective area of the electrodes. Figure 3B shows the chronocoulometric curve of the bare GCE (black) and PDDA-RGO/GCE (red) in 1 mM K$_3$Fe(CN)$_6$ containing 0.1 M KCl. The electroactive surface area can be calculated as follow [47]:

$$Q = \frac{2nFAcD^{1/2}t^{1/2}}{\pi^{1/2}} + Q_{dl} + Q_{ads}$$

Where A (cm^2) is the electrode surface area, D (cm^2/s) is the diffusion coefficient of the Fe(CN)$_6$$^{3-}$, c (mol cm^{-3}) is the bulk concentration of the Fe(CN)$_6$$^{3-}$, t (s) is the potential pulse width, Q$_{dl}$ (C) is the double-layer charge, Q$_{ads}$ (C) is the Faradaic charge due to the oxidation of adsorbed Fe(CN)$_6$$^{3-}$. The slope of the Q–t$^{1/2}$ plots can be expressed as 2nFAcD$^{1/2}$/$\pi^{1/2}$. According to the literature, the n and D for K$_3$Fe(CN)$_6$ is 1 and 7.6 × 10^{-6} cm^{-1}/s [48]. The electroactive surface areas of the the bare GCE and PDDA-RGO/GCE are calculated to be 0.1107 and 0.4711 cm^2, respectively.

3.2 Electrochemical behavior of luteolin at PDDA-RGO nanosheet modified electrodes

Figure 4A shows the voltammetric response of different electrodes towards detection of 10 μM luteolin in PBS of pH 5.0 at scan rate of 50 mV/s. As shown in Figure 4A, there is no redox peak at PDDA-RGO/GCE without luteolin (curve b), indicating that PDDA-RGO/GCE is non-electroactive in the selected potential range. However, bare GCE, RGO/GCE and PDDA-RGO/GCE all show a couple of redox peaks when the presence of 10 μM luteolin, revealing that luteolin undergoes a quasi-reversible redox process on the electrode. At bare GCE (curve a), a pair of poor redox peaks are obtained. While at RGO modified GCE (curve c), the current responses of luteolin are significantly increased compared with the bare GCE. This current response enhancement could ascribe to the excellent conductivity and high surface area of RGO sheets. The PDDA-RGO/GCE shows a similar CV profile but with a higher current response, which indicates that the PDDA surface functionalization of RGO can further enhance the catalyzed redox of luteolin. Moreover, the anodic and cathodic peak potential of luteolin shift to negative and positive values relative to those obtained by RGO/GCE and bare GCE, indicating the PDDA-RGO modification can increase the reversibility of the electrode and reducing the overpotential for electrooxidation of luteolin.

The peak potentials and the peak currents are closely linked to the pH of PBS. Figure 4B shows the CVs of redox of luteolin using PDDA-RGO/GCE in different pH conditions. As shown in Figure

4C, the anodic and cathodic peak current of luteolin increases gradually with increasing the pH up to 5.0, and the maximum peak current is obtained at pH 5.0. With further increasing pH, the oxidation peak current conversely decreases due to the shortage of proton [20].
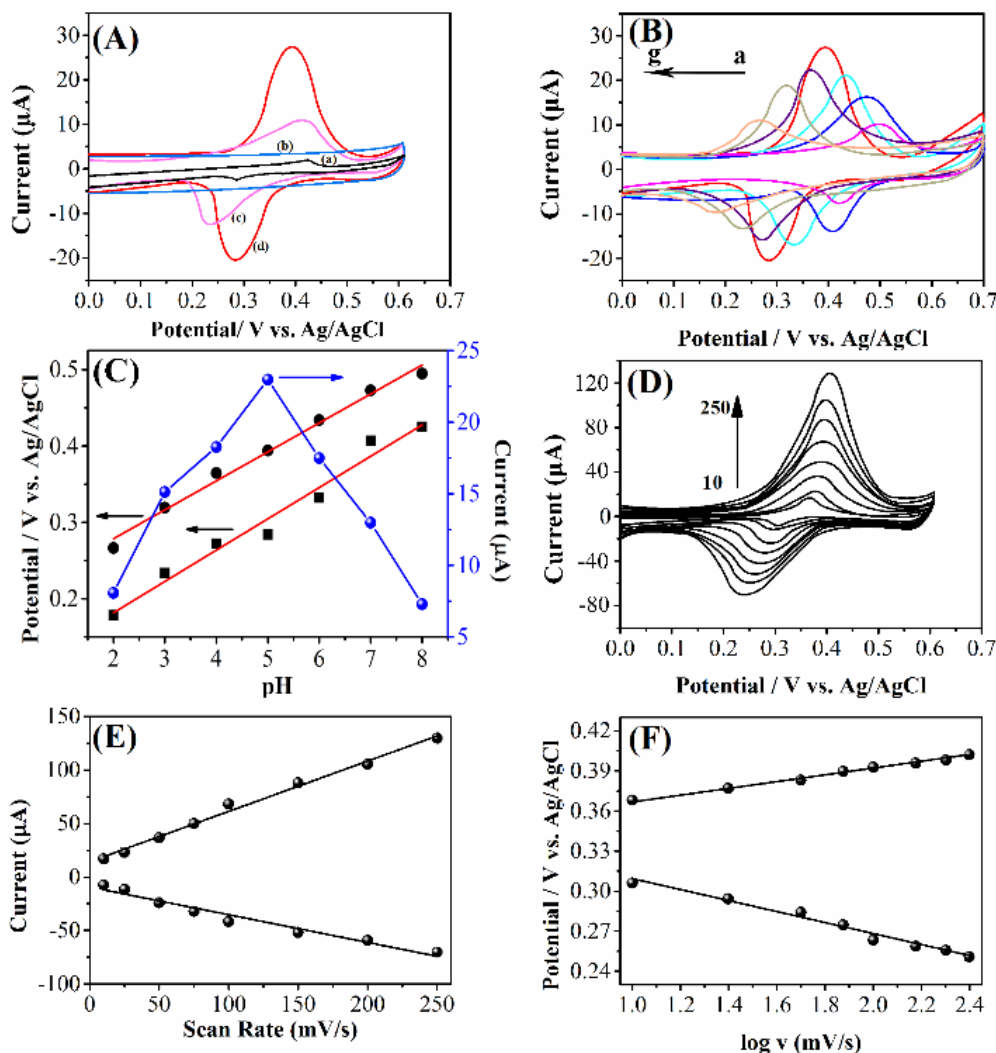

Figure 4. (A) CVs of bare (a) GCE, (c) RGO (b, d) PDDA-RGO modified GCEs in 0.1 M PBS (pH 5.0) absence and presence of 10 µM luteolin. Scan rate: 50 mV/s. (B) CVs of PDDA-RGO modified GCE in 10 µM luteolin at different pH conditions (a to g: 2, 3, 4, 5). (C) Effect of pH on the oxidation current and oxidation potential. (D) CVs of PDDA-RGO modified GCE in 10 µM luteolin at different scan rates (10, 25, 50, 75, 100, 150, 200, 250 mV/s). (E) The plot for the dependence of peak current on scan rate. (F) The relationship between redox potential and log v.

Therefore, pH 5.0 was selected as the optimum pH for the further studies. Moreover, when the pH changes from 2.0 to 8.0, the anodic and the cathodic peak potential shift to the negative direction. The linear shift of oxidation and reduction toward the negative potential with an increasing pH indicated that protons were directly involved in the redox of luteolin. The linear regression equation can be represented as: E_{pa} (V) = 0.05784 pH + 0.20269 (R^2 = 0.992); E_{pc} (V) = 0.0521 pH + 0.09974

(R^2 = 0.987). A slopes of d_{Ep}/d_{pH} plots are close to the theoretical value of 60 mV per pH unit, indicating the electron transfer of luteolin redox is accompanied by an equal number of electrons and protons [19, 21].

Figure 4D displays the CVs of 10 μM luteolin at PDDA-RGO/GCE with different scan rates. It can be seen that the redox peak currents increase gradually with the increase of scan rate in the ranged from 10 to 250 mV/s, accompanied with an enlargement of the peak separation. Linear relationships are obtained between the peak currents and the scan rates (Figure 4E). The linear regression equations are: I_{pa} (μA) = 0.47025 v (mV/s) + 14.27291 0(R^2 =0.991) and I_{pc} (μA) = −0.25872 v (mV/s) − 9.46617 (R^2 =0.984), respectively. The results indicate that the process is adsorption controlled. On the other hand, the scan rate also affects the position of the redox peaks. As shown in the figure, with increasing the scan rate, the oxidation peak potential shifts positively and the reduction peak potential shifts negatively. Linear relationships are obtained between the redox potentials and the logarithm of scan rates (Figure 4F). The linear regression equations are: Epa (V) = 0.02542 log(v) (mV/s) + 0.34135 (R^2 =0.987) and E_{pc} (V) = −0.04117 log(v) (mV/s) + 0.35057 (R^2 =0.991), respectively. According to the method demonstrated by Laviron [49, 50], the slope of the line for E_{pa} and E_{pc} can be expressed as 2.3RT/(1 − α)nF and −2.3RT/αnF, respectively. Where R is the gas constant; α is the electron transfer coefficient; F is the Faraday's constant and n is the electron-transfer number. The value of the α and is determined as 0.57. Therefore, the total number of electrons involved in the redox of luteolin is found equal to 2. The possible redox mechanism has been expressed in Figure 5.
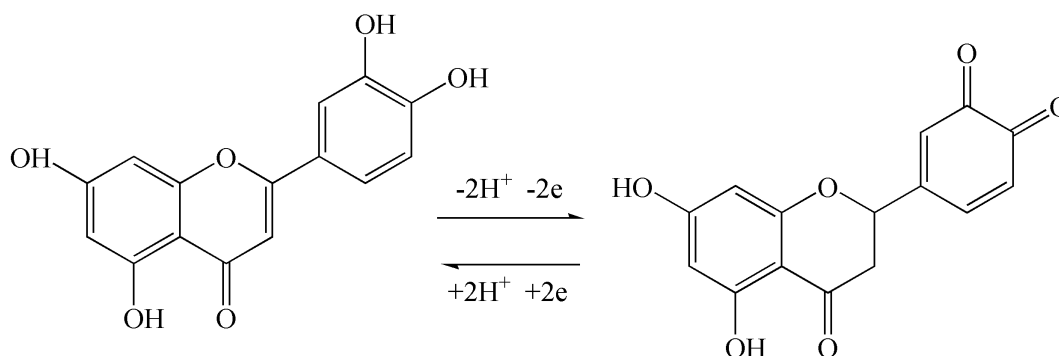

Figure 5. Electrochemical redox mechanism of luteolin.

The effect of accumulation potential and time on the anodic peak current response of luteolin was investigated as well. As shown in Figure 6A, the highest oxidation current response is obtained at 0.4 V. The peak current increases gradually with the increase of accumulation time from 0 to 120 s and remains a similar performance if a longer accumulation time is applied (Figure 6B). Therefore, the accumulation conditions of 0.4 V and 120 s were used in further measurements.

Under the optimum experimental conditions, differential pulse voltammetric (DPV) was adopted to study the anodic peak current response of luteolin on PDDA-RGO/GCE. As shown in Figure 7A, the oxidation currents gradually increase along with the increasing of luteolin concentration from 0.01 to 10 μM. Figure 7B demonstrates that the current response of PDDA-RGO/GCE is linearly related to the concentrations of luteolin. The linear regression equation is I_{pa} (μA) = 3.3167 c (μM) +

0.524, with a correlation coefficient of 0.994. The detection limit for luteolin is calculated to be 0.001 μM based on a signal-to-noise ratio of 3.
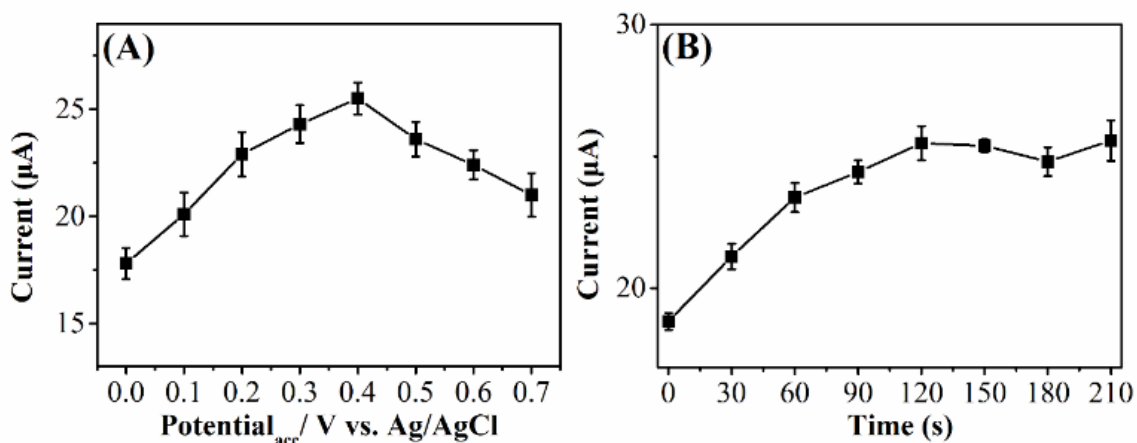

Figure 6. Effects of (A) accumulation potential and (B) time on PDDA-RGO/GCE in 10 μM luteolin (PBS = 5.0).
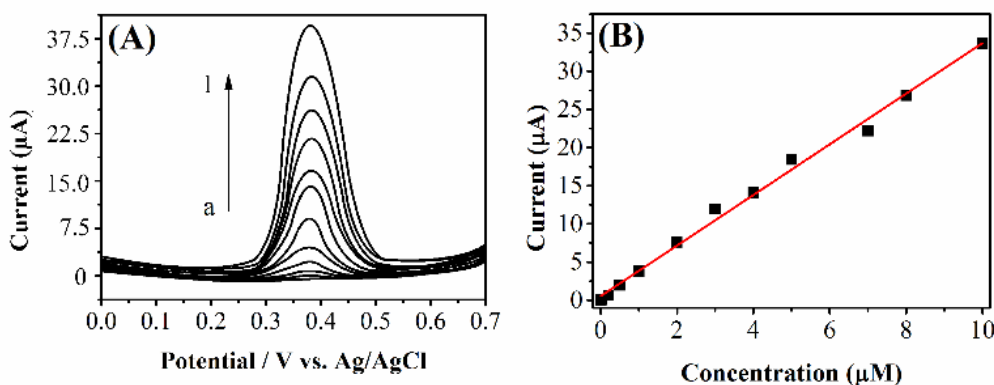

Figure 7. (A) DPV curves for luteolin at PDDA-RGO/GCE with different concentrations of luteolin (from a to k: 0.01, 0.05, 0.2, 0.5, 1.0, 2.0, 3.0, 4.0, 5.0, 7.0, 8.0, 10.0 μM). (B) Calibration curve of luteolin at the PDDA-RGO/GCE.

Table 1. Performance comparison of the proposed PDDA-RGO/GCE and sensors reported by previous reports.

Electrode	LOD (μM)	Linear range(μM)	Reference
GCE	0.005	0.3-30	[51]
Au–BMI·PF$_6$–CPE	0.028	0.1-5.8	[2]
Graphene/HA/GCE	0.01	0.02-10	[20]
Cu/Graphene/GCE	0.03	0.7-3	[52]
macroporous carbon/GCE	0.0013	0.3-30	[21]
PDDA-RGO/GCE	0.001	0.01-10	This work

Table 1 shows the comparison of analytical performances of this luteolin sensor with other luteolin sensors reported previously.

The effect of some interference species on the determination of luteolin was also investigated under the optimum experimental conditions. It was found that 100-fold concentrations of inorganic ions of K^+, Ca^{2+}, Mg^{2+}, Cu^{2+}, Na^+, Fe^{3+}, SO_4^{2-}, NO_3^-, Cl^- and 50-fold concentrations of ascorbic acid, cysteine, lysine and glucose have no influence on the signals of luteolin with the deviation below 4%. These results indicate that the proposed sensor can selectively detect the luteolin and can offer credible signal when the presence of high concentration of interfering species.

3.3 Repeatability, stability and real sample analysis

In order to test the repeatability of the PDDA-RGO/GCE, a 10 μM luteolin solution was successively measured for 10 times using the proposed sensor. The RSD values were found to be 1.52% for the analyte. Six fresh fabricated PDDA-RGO/GCEs were also used for determining 10 μM luteolin solution. The RSD was calculated to be 2.71 %. The storage stability also was tested by storing the modified GCE in refrigerator at 4°C for 3 weeks. The results show that the oxidation peak potential of luteolin had no shift and the current response only showed 2.77% decrease compared with the original test. Therefore, the luteolin sensor fabricated by PDDA-RGO/GCE exhibited a satisfactory reproducibility precision and stability.

In order to evaluate the practical performance of the proposed sensor, the fabricated PDDA-RGO/GCE was used to determine luteolin in thyme. Thyme was purchased from the local nursery. The sample was washed and chopped to small species. The sample is then boiled in 30 mL of ethanol for 15 min. After cooling, the extract was filtered, centrifuged and stored in refrigerator. The standard addition method was then applied, by adding successive concentrations of luteolin. As shown in Table 2, the recovery for the determination of luteolin was in the range of 98.2–101.3%. Therefore, the proposed luteolin sensor could be employed for practical determining luteolin concentration in real samples.

Table 2. Determination of luteolin in thyme.

Sample	Added (μM)	Found (μM)	Recovery (%)	RSD (%)
1	0	1.19	—	4.15
2	2	3.21	100.6	2.31
3	5	6.27	101.3	1.61
4	8	9.02	98.2	2.22

4. CONCLUSION

In this study, a simple wet chemical method was adopted for surface functionalization of RGO using PDDA. The synthesized PPDA-RGO sheets were characterized by SEM, XRD, Raman

spectroscopy, UV-vis spectroscopy, FTIR and electrochemical methods, and then employed successfully in the sensitive electrochemical determination of luteolin. The PDDA-RGO modified GCE displays a wide detection linear range (0.01 µM to 10 µM) and low detection limit (0.001 µM) for luteolin sensing. This study demonstrates that the surface functionalized RGO sheets is an effective approach for designing high performance electrochemical sensors.

Reference

1. M.L. Neuhouser, *Nutrition and Cancer*, 50 (2004) 1
2. A.C. Franzoi, I.C. Vieira, J. Dupont, C.W. ScheerenandL.F. de Oliveira, *The Analyst*, 134 (2009) 2320
3. E. Middleton JrandC. Kandaswami, *Biochemical Pharmacology*, 43 (1992) 1167
4. N.C. CookandS. Samman, *The Journal of Nutritional Biochemistry*, 7 (1996) 66
5. M.T. Fernandez, M.L. Mira, M.H. FlorêncioandK.R. Jennings, *Journal of Inorganic Biochemistry*, 92 (2002) 105
6. Y.J. Park, H.J. Kim, S.J. Lee, H.-Y. Choi, C. JinandY.S. Lee, *Chemical and Pharmaceutical Bulletin*, 55 (2007) 1065
7. J.K. Lee, S.Y. Kim, Y.S. Kim, W.-H. Lee, D.H. HwangandJ.Y. Lee, *Biochemical Pharmacology*, 77 (2009) 1391
8. K. Kanazawa, M. Uehara, H. YanagitaniandT. Hashimoto, *Archives of Biochemistry and Biophysics*, 455 (2006) 197
9. G. Cao, E. SoficandR.L. Prior, *Free Radical Biology and Medicine*, 22 (1997) 749
10. F.M. Areias, P. Valentão, P.B. Andrade, F. FerreresandR.M. Seabra, *Food Chemistry*, 73 (2001) 307
11. L. Li, H. Jiang, H. WuandS. Zeng, *Journal of Pharmaceutical and Biomedical Analysis*, 37 (2005) 615
12. S.n.A.O. Santos, C.S.R. Freire, M.R.r.M. Domingues, A.J.D. SilvestreandC.P. Neto, *Journal of Agricultural and Food Chemistry*, 59 (2011) 9386
13. Y.-Y. Li, Q.-F. Zhang, H. Sun, N.-K. CheungandH.-Y. Cheung, *Talanta*, 105 (2013) 393
14. Y. Peng, J. YeandJ. Kong, *Journal of Agricultural and Food Chemistry*, 53 (2005) 8141
15. I. BaranowskaandD. Raróg, *Talanta*, 55 (2001) 209
16. C.S. Liu, Y.S. Song, K.J. Zhang, J.C. Ryu, M. KimandT.H. Zhou, *Journal of Pharmaceutical and Biomedical Analysis*, 13 (1995) 1409
17. D. Lu, S. Lin, L. Wang, T. Li, C. WangandY. Zhang, *Journal of Solid State Electrochemistry*, 18 (2014) 269
18. A.Y. Tesio, A.M. Granero, N.R. Vettorazzi, N.F. Ferreyra, G.A. Rivas, H. FernándezandM.A. Zon, *Microchemical Journal*, 115 (2014) 100
19. D. Zhao, X. Zhang, L. Feng, Q. QianandS. Wang, *Food Chem*, 127 (2011) 694
20. P. Pang, Y. Liu, Y. Zhang, Y. GaoandQ. Hu, *Sensors and Actuators B: Chemical*, 194 (2014) 397
21. L. Zeng, Y. Zhang, H. WangandL. Guo, *Analytical Methods*, 5 (2013) 3365
22. L. Wu, Y. Gao, J. Xu, L. LuandT. Nie, *Electroanalysis*, 26 (2014) 2207
23. C.-H. Lu, H.-H. Yang, C.-L. Zhu, X. ChenandG.-N. Chen, *Angewandte Chemie International Edition*, 48 (2009) 4785
24. L. Fu, W. Cai, A. WangandY. Zheng, *Materials Letters*, 142 (2015) 201
25. L. FuandZ. Fu, *Ceram Int*, 41 (2015) 2492
26. A. Wang, H.P. Ng, Y. Xu, Y. Li, Y. Zheng, J. Yu, F. Han, F. PengandL. Fu, *Journal of Nanomaterials*, 2014 (2014) 6

27. L. Fu, A. Wang, Y. Zheng, W. CaiandZ. Fu, *Materials Letters*, 142 (2015) 119
28. F. Xu, M. Deng, Y. Liu, X. Ling, X. DengandL. Wang, *Electrochemistry Communications*, 47 (2014) 33
29. W.S. HummersandR.E. Offeman, *Journal of the American Chemical Society*, 80 (1958) 1339
30. T. GanandS. Hu, *Microchim Acta*, 175 (2011) 1
31. Y. Xue, H. Zhao, Z. Wu, X. Li, Y. HeandZ. Yuan, *Biosensors and Bioelectronics*, 29 (2011) 102
32. T. Nakajima, A. MabuchiandR. Hagiwara, *Carbon*, 26 (1988) 357
33. D. Miao, J. Li, R. Yang, J. Qu, L. QuandP.d.B. Harrington, *Journal of Electroanalytical Chemistry*, 732 (2014) 17
34. L. Fu, Y. Zheng, Q. Ren, A. WangandB. Deng, *Journal of Ovonic Research*, 11 (2015) 21
35. Z.-J. Fan, W. Kai, J. Yan, T. Wei, L.-J. Zhi, J. Feng, Y.-m. Ren, L.-P. SongandF. Wei, *ACS Nano*, 5 (2010) 191
36. L.L. Zhang, R. ZhouandX.S. Zhao, *Journal of Materials Chemistry*, 20 (2010) 5983
37. S. Wang, D. Yu, L. Dai, D.W. ChangandJ.-B. Baek, *ACS Nano*, 5 (2011) 6202
38. A.M. Rao, P.C. Eklund, S. Bandow, A. ThessandR.E. Smalley, *Nature*, 388 (1997) 257
39. X. Qi, K.-Y. Pu, X. Zhou, H. Li, B. Liu, F. Boey, W. HuangandH. Zhang, *Small*, 6 (2010) 663
40. M.-C. Hsiao, S.-H. Liao, M.-Y. Yen, P.-I. Liu, N.-W. Pu, C.-A. WangandC.-C.M. Ma, *ACS applied materials & interfaces*, 2 (2010) 3092
41. J.I. Paredes, S. Villar-Rodil, A. Martínez-AlonsoandJ.M.D. Tascón, *Langmuir*, 24 (2008) 10560
42. D. Li, M.B. Muller, S. Gilje, R.B. KanerandG.G. Wallace, *Nat Nano*, 3 (2008) 101
43. J. Zhang, H. Yang, G. Shen, P. Cheng, J. ZhangandS. Guo, *Chemical Communications*, 46 (2010) 1112
44. M. Ahmad, E. Ahmed, Z.L. Hong, J.F. Xu, N.R. Khalid, A. ElhissiandW. Ahmed, *Appl Surf Sci*, 274 (2013) 273
45. X. Li, Q. Wang, Y. Zhao, W. Wu, J. ChenandH. Meng, *Journal of colloid and interface science*, 411 (2013) 69
46. L.-j. Liu, X. Gao, P. Zhang, S.-l. Feng, F.-d. Hu, Y.-d. LiandC.-m. Wang, *Journal of Analytical Methods in Chemistry*, 2014 (2014) 9
47. F.C. Anson, *Analytical Chemistry*, 36 (1964) 932
48. A.J. BardandL.R. Faulkner, Electrochemical Methods: Fundamentals and Applications, 2nd Edition, Wiley1980.
49. E. Laviron, *J. Electroanal. Chem.*, 101 (1979) 19
50. E. Laviron, *J. Electroanal. Chem.*, 52 (1974) 355
51. A. Liu, S. Zhang, L. Huang, Y. Cao, H. Yao, W. ChenandX. Lin, *Chemical & Pharmaceutical Bulletin*, 56 (2008) 745
52. T. YangandD. Jiang, *Asian Journal of Chemistry*, 25 (2013) 8388